ISSN 1812-5123. Russian Journal of Biomechanics. 2013. Vol. 17, No. 4 (62): 75-94

Russian Journal of Biomechanics
www.biomech.ru

NONAXISYMMETRIC MATHEMATICAL MODEL OF THE CARDIAC LEFT VENTRICLE ANATOMY

S.F. Pravdin[1, 2, 3]

[1] Department of Function Approximation Theory, Institute of Mathematics and Mechanics, Ural Branch of Russian Academy of Science, 620990, Ekaterinburg, 16 S. Kovalevskaya Street, e-mail: sfpravdin@imm.uran.ru
[2] Laboratory of Mathematical Physiology, Institute of Immunology and Physiology, Ural Branch of Russian Academy of Science, 620041, Ekaterinburg, 106 Pervomayskaya Street
[3] Physics and Astronomy Department, Faculty of Sciences, University of Ghent, 25 Sint-Pietersnieuwstraat, B-9000, Gent, Belgium

Abstract. We describe a mathematical model of the shape and fibre direction field of the cardiac left ventricle. The ventricle is composed of surfaces which model myocardial sheets. On each surface, we construct a set of curves corresponding to myocardial fibres. Tangents to these curves form the myofibres direction field. The fibres are made as images of semicircle chords parallel to its diameter. To specify the left ventricle shape, we use a special coordinate system where the left ventricle boundaries are coordinate surfaces. We propose an analytic mapping from the semicircle to the special coordinate system. The model is correlated with Torrent-Guasp's concept of the unique muscular band and with Pettigrew's idea of nested surfaces. Subsequently, two models of concrete normal canine and human left ventricles are constructed based on experimental Diffusion Tensor Magnetic Resonance Imaging data. The input data for the models is only the left ventricle shape. In a local coordinate system connected with the left ventricle meridional section, we calculate two fibre inclination angles, i.e. true fibre angle and helix angle. We obtained the angles found from the Diffusion Tensor Magnetic Resonance Imaging data and compared them with the model angles. We give the angle plots and show that the model adequately reproduces the fibre architecture in the majority of the left ventricle wall. Based on the mathematical model proposed, one can construct a numerical mesh that makes it possible to solve electrophysiological and mechanical left ventricle activity problems in norm and pathology. In the special coordinate system mentioned, the numerical scheme is written in a rectangular area and the boundary conditions can simply be written. By changing the model parameters, one can set a general or regional ventricular wall thickening or the left ventricle shape change, which is typical for certain cardiac pathologies.

Keywords: left ventricle, myocardial architecture, myocardial sheets, mathematical anatomy, analytical cardiac model.

INTRODUCTION

Currently, the modelling of complex physiological systems necessitates the inclusion of a description from the molecular to whole organ level, the heart is no exception. Modern cardiac models allow researchers to study mechanisms of two main types of cardiac activity, mechanical and electrical, and to reproduce not only normal, but also pathologic conditions.

Lately, several models of electrical and/or mechanical function of the whole heart or its chambers have been described [35, 4, 10, 15, 38, 37, 9, 22, 30, 20, 17, 28].

Sergei F. Pravdin, researcher of Institute of Mathematics and Mechanics; researcher, Institute of Immunology and Physiology, Ekaterinburg; Ph.D. student of University of Gent, Belgium

Minute descriptions of the shape and fibre direction field of the heart are a key component of the most recent organ-level models.

Cardiac anatomy and anisotropy can be represented by two methods: developing individual maps, where various experimental techniques yield directly measured fibre orientation of a particular heart, and by generation the orientation field using algorithms. The latter approach is called 'theoretical', or 'rule-based'.

In 1972, Spanish cardiologist Torrent-Guasp demonstrated that the myocardium of both right and left heart ventricles can be considered a single muscular band twisted and wrapped into a double helical coil [33]. Based on this concept, a theoretical model of the left ventricle's shape and fibre orientation field was proposed [27]. This model also relies on Pettigrew's idea [24] of the left ventricle as a set of nested muscular sheets, each of which is filled by myofibres. As Pettigrew states, these sheets are evolvents of plane semicircles and images of the myofibres are chords that parallel the semicircle diameter.

For verification of the model [27], its authors used Streeter's [31] and Hunter's [21] experimental data. They showed that the model reproduced cardiac anisotropy properties such as the rotation of fibres in the left ventricle wall, dependence of the rotation on position in the wall (base-apex), spiral fibre run at the apex and maximal angle of fibre revolution round the vertical left ventricle axis. Quantitative comparison with the experimental data mentioned shows agreement between the data in the left ventricle free wall.

In [27], an axisymmetric model of the truncated left ventricle (only below the equator) is described. The present article generalizes that model. The real left ventricles of different species can have both an axisymmetric and substantially nonsymmetric form. For example, canine left ventricle can for convenience be divided into two parts, prominent free wall and interventricular septum, which significantly juts into the upper part of left ventricle cavity. In the present work, we construct a non-axisymmetric model of the left ventricle. In our model, both anatomy and fibre direction field are determined analytically.

THE LEFT VENTRICLE MODEL CONSTRUCTION

In order to determine the left ventricle form, we use a special coordinate system (γ, ψ, φ), where the variable $\gamma \in [\gamma_0, \gamma_1] \subseteq [0,1]$ corresponds to position of a point in the left ventricle wall layer, $\gamma = \gamma_0$ is the epicardium, $\gamma = \gamma_1$ is the endocardium, $\psi \in [0, \pi/2]$ is analogue of latitude, $\psi = 0$ is the upper plane part of the left ventricle model (fibrous ring and valve zone), $\psi = \pi/2$ is the left ventricle apex and $\varphi \in [0, 2\pi)$ is analogue of longitude.

We can transform the special coordinates into cylindrical ones (ρ, φ, z) using the formulae (Fig. 1):

$$\rho(\gamma,\psi,\varphi) = \rho_{inmer}\left(\psi,\, r_0^f(\varphi) - \gamma d_0^f(\varphi),\, r_e^f(\varphi) - \gamma d_e^f(\varphi),\right.$$
$$\left. l_1^f(\varphi) + \gamma\left(l_0^f(\varphi) - l_1^f(\varphi)\right),\, p(\varphi)\right), \tag{1}$$

$$z(\gamma,\psi) = Z^f - \left(Z^f - h^f\gamma\right)\sin\psi + \Delta z, \tag{2}$$

$$\rho_{inmer}(\psi, r_0, r_e, l, p) = \begin{cases} r_e - (r_e - r_0)\cdot(1 - \psi/l)^p, & \text{if } \psi < l, \\ r_e \cdot \left[1 - \left(\dfrac{\psi - l}{\pi/2 - l}\right)^p\right], & \text{otherwise,} \end{cases} \tag{3}$$

where $\rho_{inmer}(\psi, r_0, r_e, l, p)$ is coordinate ρ of a point with coordinate ψ in the left ventricle wall, if the left ventricle base has coordinates $\rho = r_0, \psi = 0$, the equator has coordinates

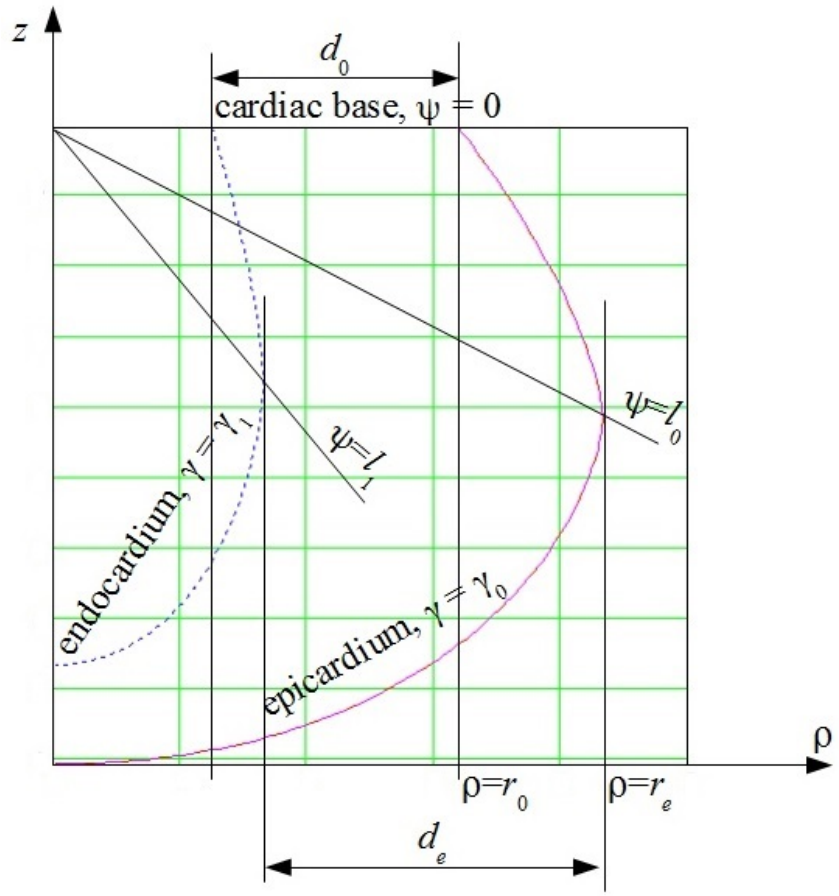

Fig. 1. A meridional section of the model

$\rho = r_e, \psi = l$ and $p > 1$; $r_{0,e}(\varphi)$ is the left ventricle epicardial radius at the base, equator; $d_{0,e}(\varphi)$ is the left ventricle epicardial wall thickness at the base, equator; $l_{0,1}(\varphi)$ is the latitude ψ of equator at the epicardium, endocardium; Z is the left ventricle height; h is the left ventricle wall thickness at the apex; $p(\varphi) > 1$; index f means formal parameter and r means real parameter;

$$r_0^f = r_0^r + d_0^r\gamma_0/(\gamma_1-\gamma_0),\ d_0^f = d_0^r/(\gamma_1-\gamma_0),\ r_e^f = r_e^r + d_e^r\gamma_0/(\gamma_1-\gamma_0),$$
$$d_e^f = d_e^r/(\gamma_1-\gamma_0),\ l_0^f = \left[(\gamma_1-1)l_1^r + (1-\gamma_0)l_0^r\right]/(\gamma_1-\gamma_0),$$
$$l_1^f = \left(\gamma_1 l_1^r - \gamma_0 l_0^r\right)/(\gamma_1-\gamma_0),\quad h^f = h^r/(\gamma_1-\gamma_0),\ Z^f = Z^r + h^r/(\gamma_1-\gamma_0),$$
$$\Delta z = -h^r\gamma_0/(\gamma_1-\gamma_0).$$

Spiral surfaces

The model of left ventricle myocardium consists of fibres that lie on spiral surfaces. An spiral surface has the following equation in the special coordinates:

$$\varphi(\gamma, \varphi_{\min}, \varphi_{\max}) = \varphi_{\min} + \gamma\varphi_{\max}, \tag{4}$$

where $\varphi_{\max}$ is the spiral surface twist angle (the same for all spiral surfaces), $\varphi_{\max}^f = \varphi_{\max}^r/(\gamma_1-\gamma_0)$, different spiral surfaces have different values of $\varphi_{\min} \in [0, 2\pi)$.

An spiral surface equation in the cylindrical coordinates (see (1), (2)):

$$\rho_{sp}\left(\psi,\varphi;\varphi_{\min}\right)=\rho\left(\frac{\varphi-\varphi_{\min}}{\varphi_{\max}},\psi,\varphi\right), \tag{5}$$

$$z_{sp}\left(\psi,\varphi;\varphi_{\min}\right)=z\left(\frac{\varphi-\varphi_{\min}}{\varphi_{\max}},\psi\right). \tag{6}$$

Filling of a spiral surface by fibres

Following J. Pettigrew's theoretical hypothesis [24] and its practical realization [25, 26, 27], we modelled myocardial fibres as images of chords with the equation Y = const, $Y\in[0, 1)$, of semicircumference P = 1; $\Phi\in[0, \pi]$ (the chords are parallel to the diameter) on the spiral surface (Fig. 2). Each chord was parameterized by the polar angle $\Phi\in[\Phi_0,\Phi_1]$, where $\Phi_0=\arcsin Y$, $\Phi_1=\pi-\arcsin Y$. Mapping of a chord point (P; Φ) to an spiral surface point is defined by the formulae (Fig. 3):

$$\gamma(\Phi)=\Phi/\pi, \tag{7}$$

$$\psi(\mathrm{P})=(1-\mathrm{P})\cdot\pi/2. \tag{8}$$

For example, image of the semicircle diameter is a fibre which begins on the epicardium, descends to the apex (Φ = π/2), then ascends and ends on the endocardium. Images of shorter chords are situated closer to the left ventricle top and have lesser length.

The left ventricle form fitting

We fitted a model of left ventricle form to one real left ventricle of a dog and of a human based on Diffusion Tensor Magnetic Resonance Imaging data, which are freely accessible online at http://gforge.icm.jhu.edu/gf/project/dtmri_data_sets/docman.

First, we found the left ventricle axis *Oz*, then we sectioned the left ventricle by N = 20 (for canine heart) or N = 24 (for human heart) meridional half-planes $\varphi_i=2\pi i/N$, i = 0, 1, …, N–1, passing over this axis, and we manually found the needed parameter values,

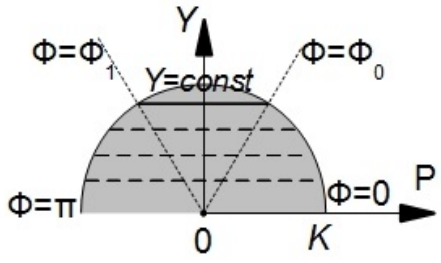

Fig. 2. Horizontal chords on the semicircle. Here, Φ_0 and Φ_1 are polar angles of the right and left chord ends

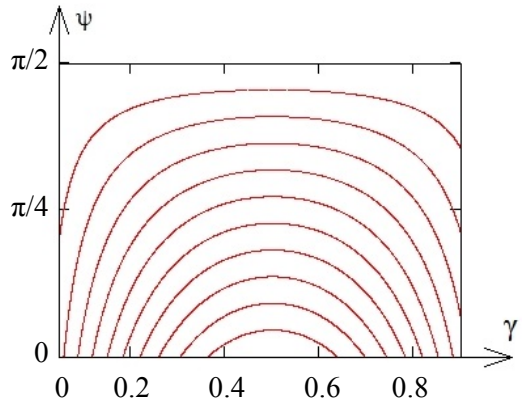

Fig. 3. Images of the semicircle chords in (γ, ψ) coordinates

ISSN 1812-5123. Russian Journal of Biomechanics. 2013. Vol. 17, No. 4 (62): 75–94

r_0, r_e, d_0, d_e, l_0, l_1, p in each section (Fig. 4, 5). After that, we found functions $r_0(\varphi)$, $r_e(\varphi)$, $d_0(\varphi)$, $d_e(\varphi)$, $l_0(\varphi)$, $l_1(\varphi)$ and $p(\varphi)$ by means of linear interpolation.

METHODS FOR THE MODEL AND EXPERIMENT COMPARISON

We related the theoretical model and experimental data by comparing the fibre slope angles that intersect normals to an epicardium meridional section. This method was described in [31] and has the following steps.

To compare angles along a normal, one needs to specify a point A on the epicardium. Let its special coordinates be $\psi = \psi_0$ and $\varphi = \varphi_0$. Let us consider a corresponding meridional section $\varphi = \varphi_0$ of the model, semiplane Π. Let us construct a normal to the epicardial section by this semiplane and find its intersection with the endocardium or the base, a point B. On the segment AB, we set k equidistant points, including its ends, so that $A = A_1, A_2, \ldots, A_k = B$. The position of a point A_i on the segment AB is defined by the variable

$$t_i = \frac{A_i B}{AB}.$$

(for the endocardium $t = 0$, for the epicardium $t = 1$). Through every point A_i, we have to draw an spiral surface. Problem of finding such an spiral surface reduces to solving a system of two algebraic equations with two unknown quantities ψ and $\varphi_{\min}$:

$$\begin{cases} \rho_{sp}(\psi, \varphi_0; \varphi_{\min}) = \rho_i, \\ z_{sp}(\psi, \varphi_0; \varphi_{\min}) = z_i, \end{cases}$$

where (ρ_i, φ_0, z_i) are cylindrical coordinates of point A_i. This problem is equivalent to conversion of cylindrical coordinates into special ones, i.e. solving system

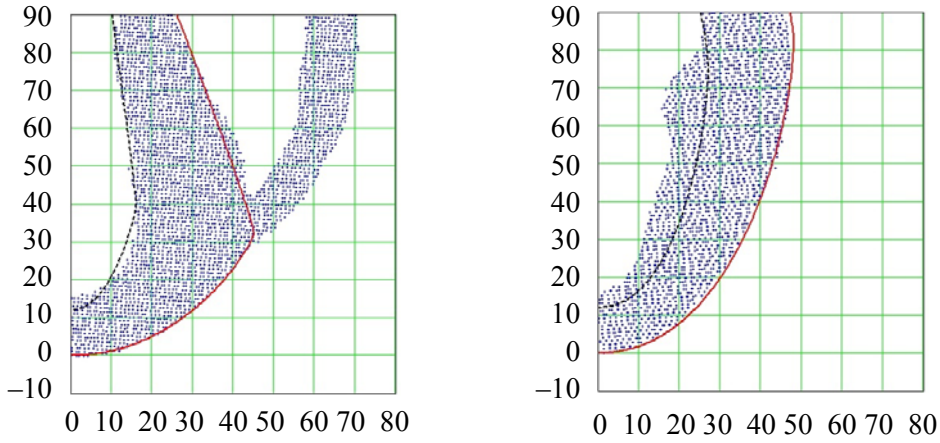

Fig. 4. Vertical (meridional) sections of the interventricular septum (on the left) and left ventricle free wall (on the right) of a canine heart. The points are Diffusion Tensor Magnetic Resonance Imaging data, the solid line is the model epicardium, the dashed line is the model endocardium. On the left panel: left ventricle cavity is to the left, the right ventricle cavity and free wall are to the right of the interventricular septum

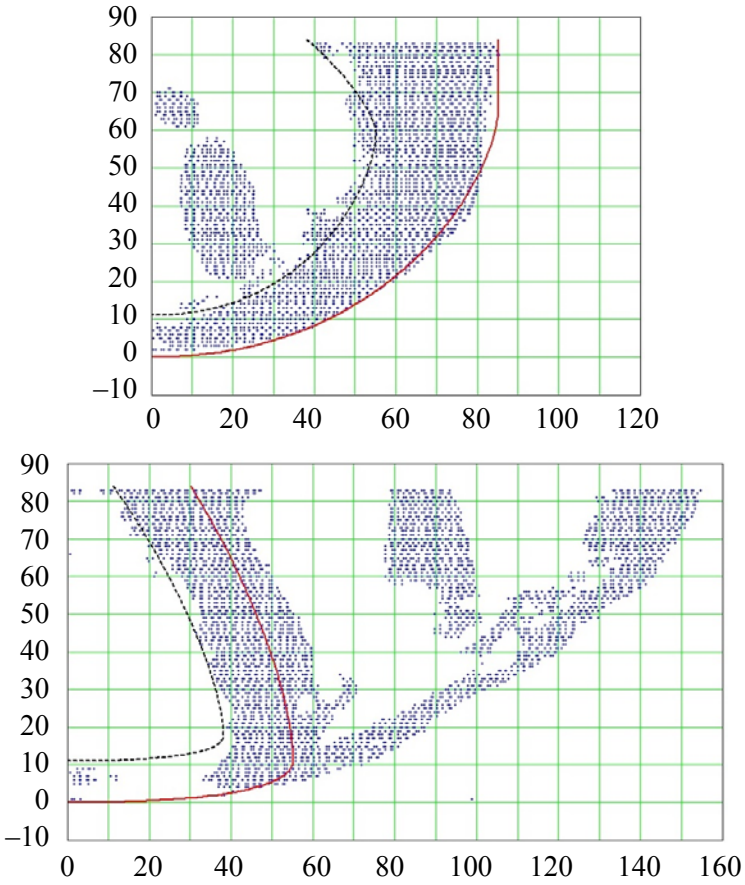

Fig. 5. Vertical (meridional) sections of the left ventricle free wall (on top) and interventricular septum (below) of a human heart. The points are Diffusion Tensor Magnetic Resonance Imaging data, the solid line is the model epicardium and the dashed line is the model endocardium. On bottom of the panel, there are papillary muscles in the right ventricle cavity (vertical one, $\rho = 80 \ldots 100$ mm) and a right ventricle free wall (inclined)

$$\begin{cases} \rho(\gamma, \psi, \varphi_0) = \rho_i, \\ z(\gamma, \psi) = z_i \end{cases}$$

with respect to ψ и γ. One can express (see (2)) ψ from the second equation of this system:

$$\psi(z_i, \gamma) = \arcsin\left(\frac{Z^f - z_i + \Delta z}{Z^f - h^f \gamma}\right) \tag{9}$$

and substitute this expression to the first equation. Then, the problem reduces to solving one nonlinear equation

$$\rho(\gamma, \psi(z_i, \gamma), \varphi_0) = \rho_i$$

with one unknown quantity γ on segment $[\gamma_0, \gamma_1]$, which can easily be done, for example, by the method of tangents.

Strictly speaking, there can be no points from the tomogram exactly on semiplane Π; therefore, we selected points lying no further than Δ = 1 mm from the straight line *AB* and inside the dihedral angle $|\varphi - \varphi_0| \le \Delta_\varphi = 0.1 \text{ rad} = 5.7^\circ$.

In his work [31], Streeter proposed specifying fibre direction using a local coordinate system (u, v, w) and two angles, 'true fibre angle' α and 'helix angle' α_1 (these angles are sufficient for specifying a fibre direction in a point). The axis u is a normal to the epicardium pointed from the left ventricle; w is a meridian, i.e. an epicardial tangent lying in a meridional semiplane and pointed upwards; v is a parallel, i.e. vector $\mathbf{w}\times\mathbf{u}$. Angle $\alpha\in[0; \pi/2]$ is an angle between a fibre and a parallel, and angle $\alpha_1 \in [-\pi/2, \pi/2]$ is an angle between fibre projection on the plane uv and a parallel.

We compared two these angular characteristics of the fibre direction field with experimental data. The comparison was conducted along epicardial normals in two meridians (one meridian lies in the left ventricle free wall, another one lies in the interventricular septum) in upper, middle and lower parts of the left ventricle wall.

RESULTS OF A COMPARISON WITH CANINE HEART DATA

The following parameter values were used: left ventricle height $Z^r = 90$ mm, left ventricle wall thickness at the apex $h^r = 12$ mm, spiral surface effective twisting angle $\varphi^r_{\max} = 3\pi$, subepicardial lamination parameter $\gamma_0 = 0.05$, subendocardial lamination parameter $\gamma_1 = 0.98$.

In Fig. 6, we show an spiral surface made using these parameter values, with chord images on it.

The comparison was conducted in different left ventricle zones: upper (epicardial normal was constructed in a point with coordinate ψ = 5°), middle (ψ = 35°) and lower one (ψ = 65°).

In Figs. 7–12, we display heart areas where we compared fibre slope angles and graphs of these angles from the experimental data (points) and from the model (solid lines). Let us analyse each figure in more detail.

At the upper part of the left ventricle free wall (Fig. 7), we see qualitative and good quantitative data agreement: angle α is maximal at the endocardium, decreases approximately to 10° at the middle of the wall, then increases and has its local maximum at the epicardium. In panel *D*, if we move from the endocardium to the epicardium, helix angle α_1 almost linearly decreases from big positive values to great in magnitude negative values and equals zero at the middle of the wall.

Similar behaviour of the angles can be observed at the middle (by height) part of the left ventricle free wall (Fig. 8). In comparison with the previous figure, both in the experiment and in the model, we notice that angle α graphs have a form close to a *V*-shape at the basal

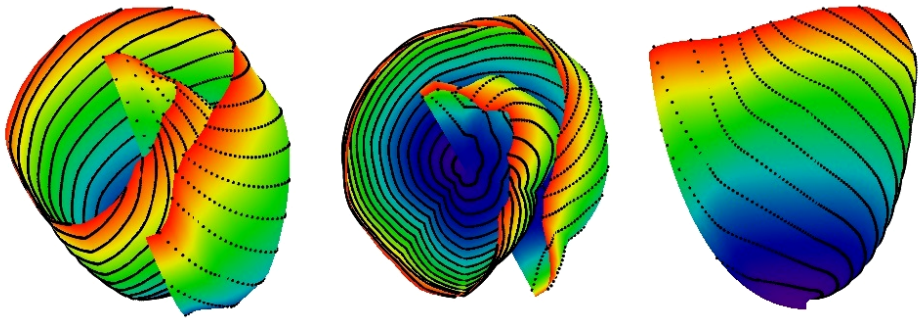

Fig. 6. An spiral surface used in the human left ventricle model with chord images on it. On the left: side and top view. At the middle: top view. On the right: side and slightly bottom view

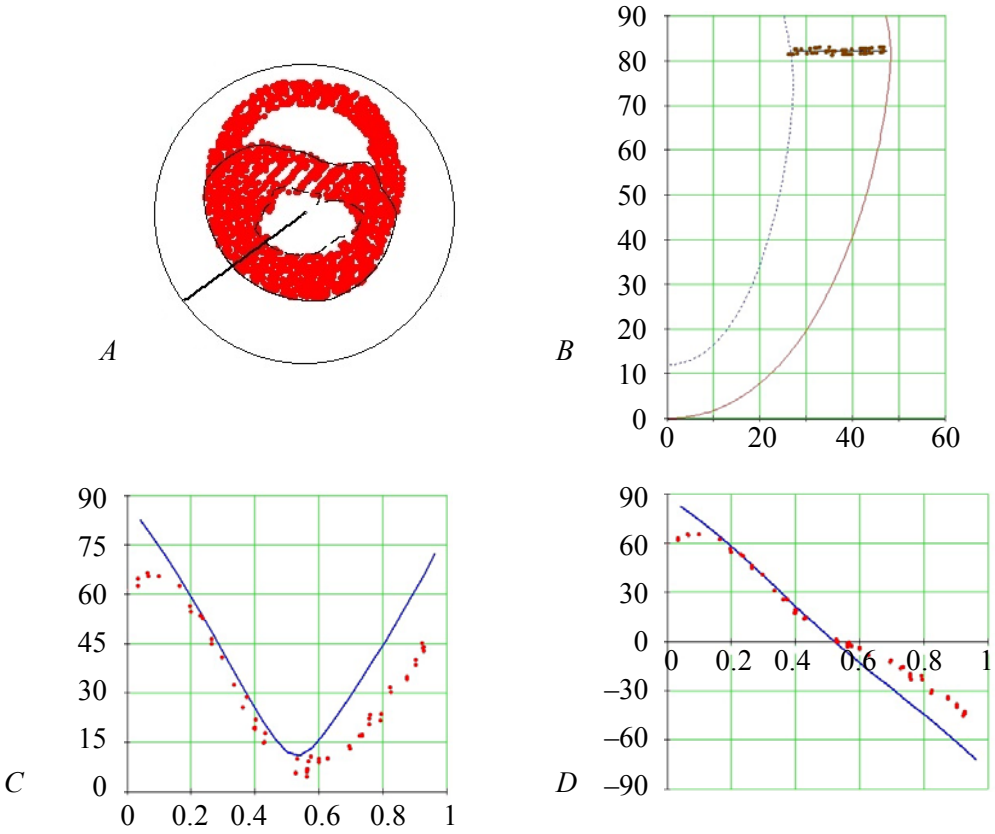

Fig. 7. The fibre angles in the model and in the experimental data. The left ventricle free wall, basal area ($\psi = 5°$), canine heart. *A* is a horizontal left ventricle section. The points are myocardial points from a Diffusion Tensor Magnetic Resonance Imaging scan, the straight line is a normal to the epicardium, the solid (dashed) curve is the model epicardium (endocardium). *B* is a meridional left ventricle section. The solid (dashed) curve is the model epicardium (endocardium) and the points are myocardial points from a Diffusion Tensor Magnetic Resonance Imaging scan. *C* shows the angle α, *D* shows the angle α_1. The *X* axis displays point position in the wall depth; 0 corresponds to the endocardium, 1 corresponds to the epicardium

area and close to *U*-shape at the middle area. Angle α_1 graph in Fig. 7 seems to be a straight line, and, in Fig. 8, it is somewhat similar to an overturned cubic parabola (i.e. at the middle of the wall the angle's decrease becomes slower; at the external and internal parts of the wall, it becomes faster).

At the apical zone (Fig. 9), the quantitative data agreement worsens, but the qualitative agreement remains. Notice that angle α_1 graphs in the model and in the experiment have come even closer to an overturned cubic parabola.

Let us now consider the interventricular septum and compare the fibre angles along three epicardial normals.

At the basal (Fig. 10), middle (Fig. 11) and apical (Fig. 12) zones, only qualitative data agreement can be observed. As at the free wall, the true fibre angle α is maximal at the endocardium, then it drops reaching its minimum at the middle of free wall and rises to have its maximum at the epicardium. Notice that in experiment and in the model, the endocardial value of this angle is greater than its epicardial value at the middle and – especially – at the lower interventricular septum part.

The helix angle α_1 decreases monotonically at the interventricular septum and at the left ventricle free wall from approximately 80° on the endocardium to –60° on the epicardium.

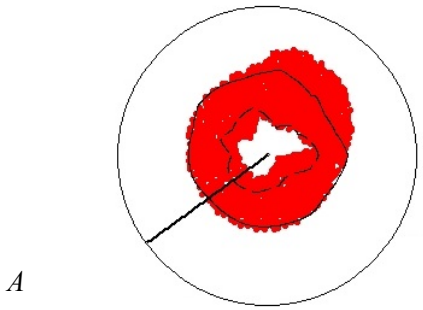

A

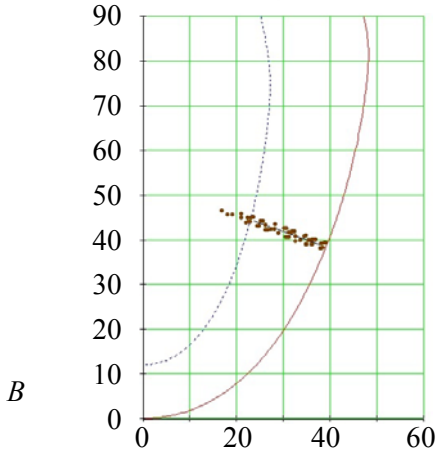

B

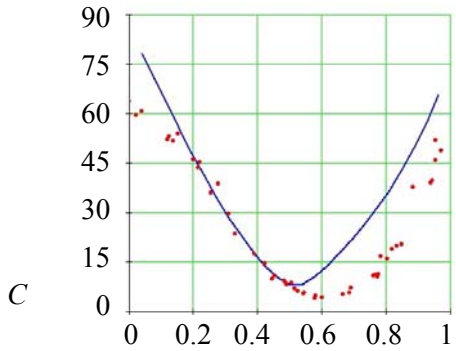

C

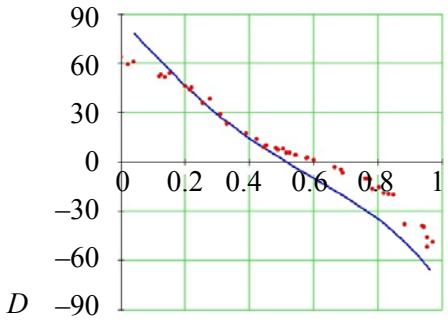

D

Fig. 8. Fibre angles in the model and in the experimental data. The left ventricle free wall, middle height area (ψ = 35°), canine heart. The conventional signs are the same as in Fig. 7

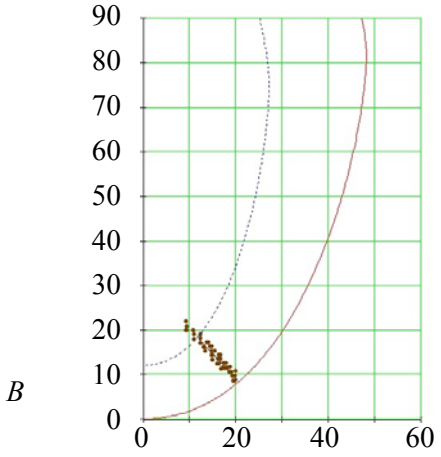

B

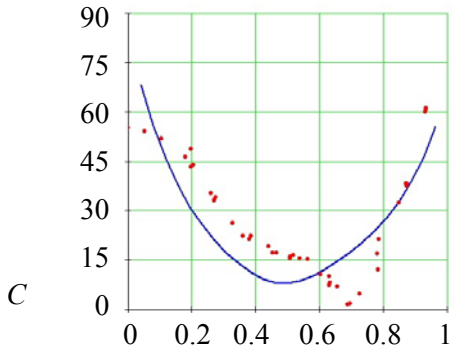

C

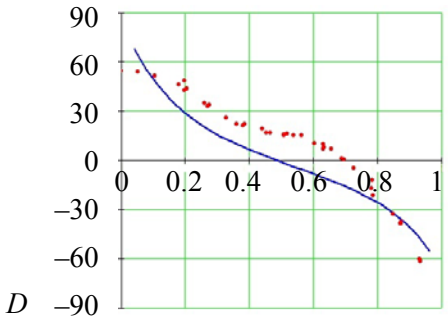

D

Fig. 9. Fibre angles in the model and in the experimental data. The left ventricle free wall, apical area (ψ = 65°), canine heart. The conventional signs are the same as in Fig. 7. Horizontal section is not shown

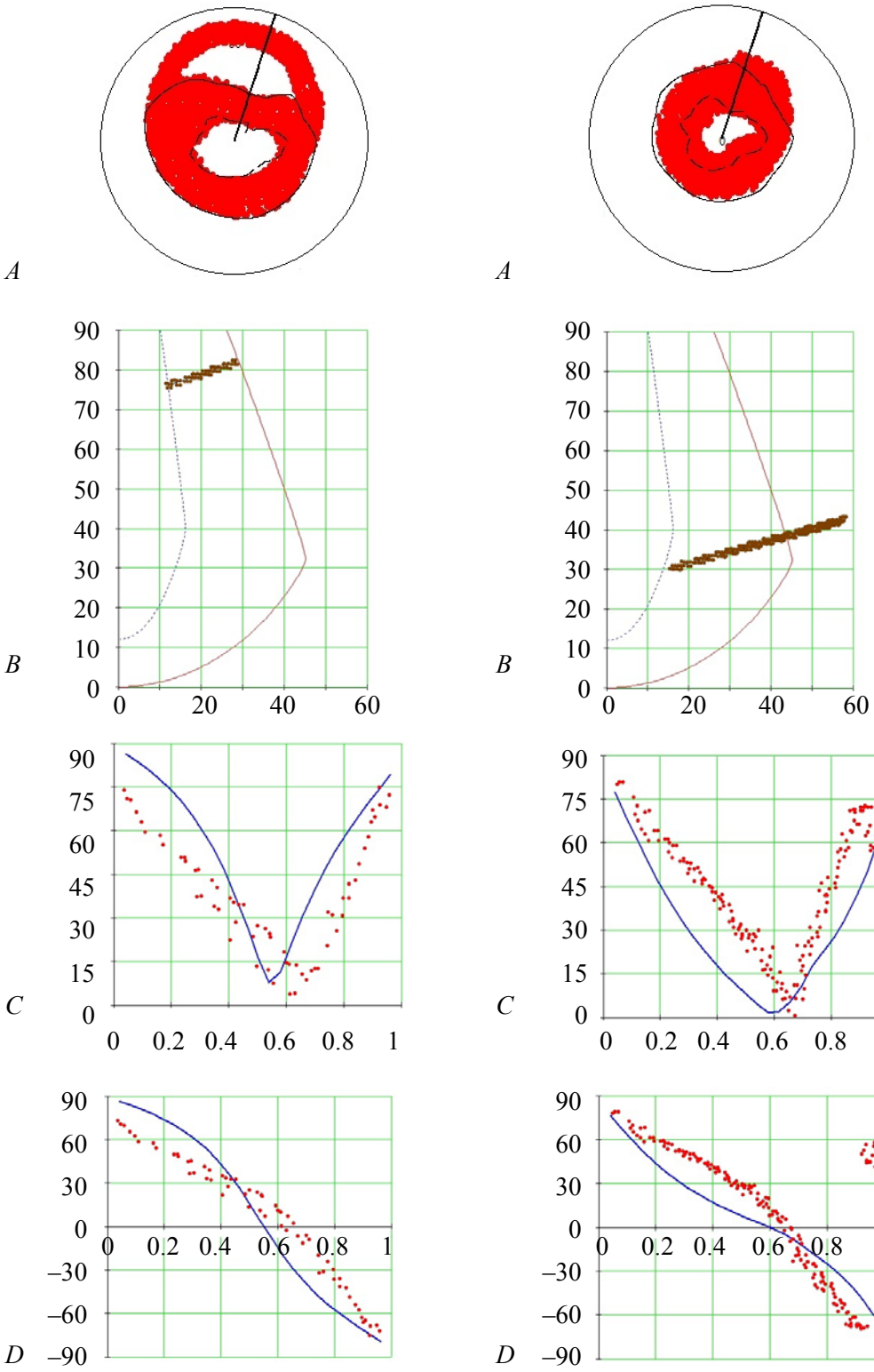

Fig. 10. The fibre angles in the model and in the experimental data. The interventricular septum, basal area ($\psi = 5°$), canine heart. The conventional signs are the same as in Fig. 7

Fig. 11. The fibre angles in the model and in the experimental data. The interventricular septum, middle height area ($\psi = 35°$), canine heart. The conventional signs are the same as in Fig. 7

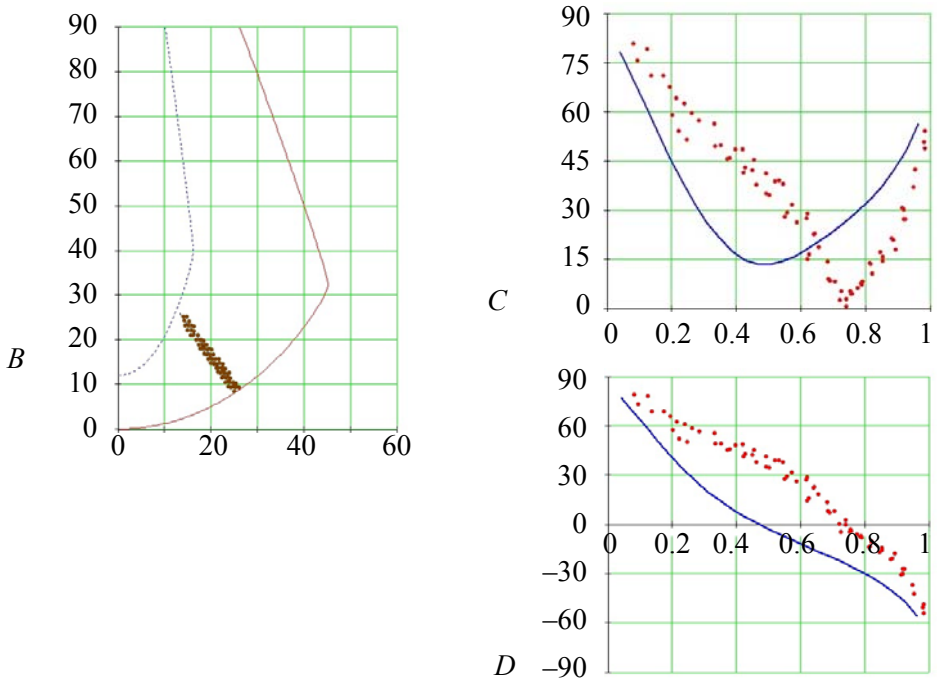

Fig. 12. The fibre angles in the model and in the experimental data. The interventricular septum, apical area ($\psi = 65°$), canine heart. The conventional signs are the same as in Fig. 7. Horizontal section is not shown

RESULTS OF A COMPARISON WITH HUMAN HEART DATA

We followed the method used to compare angles in the canine heart.

The following parameter values (common for all meridians) were used: left ventricle height $Z^r = 84$ mm, left ventricle wall thickness at the apex $h^r = 11$ mm, spiral surface effective twisting angle $\varphi^r_{max} = 2\pi$, subepicardial lamination parameter $\gamma_0 = 0.05$, subendocardial lamination parameter $\gamma_1 = 0.98$.

Graphs of dependence of angles α, α_1 on a point position on normal to the epicardium are shown in Figs. 13–18. Let us analyse the results obtained.

At the upper and middle left ventricle areas (e.g., Figs. 13 and 14, *A*), one can see that the vertical axis goes not through the centre of horizontal left ventricle sections, but is situated closer to the interventricular septum. The axis position is set there because the axis must intersect the apical left ventricle area, and the left ventricle apex projection to its basal plane is not situated at the centre of the base. If one moves the axis to the base centre, then the apex is far from the axis in one of the meridional sections; therefore, we cannot fit the left ventricle wall shape by this model.

Let us consider the fibre slope angles in one of the left ventricle free wall meridians.

In the upper left ventricle part (Fig. 13), the true fibre angle α (panel *C*) in the model rather accurately reproduces the Diffusion Tensor Magnetic Resonance Imaging data. It descends from 90° on the endocardium to approximately 25° at the middle of the wall, then it grows and reaches 70° on the epicardium. The helix angle (panel *D*) in the model is also rather close to the experimental data.

The middle (by height) part of the free wall (Fig. 14) shows an essentially large dispersion of the both angles values. At the same time, their behaviour here and in the basal zone is mostly the same, and the model can reproduce this both qualitatively and quantitatively.

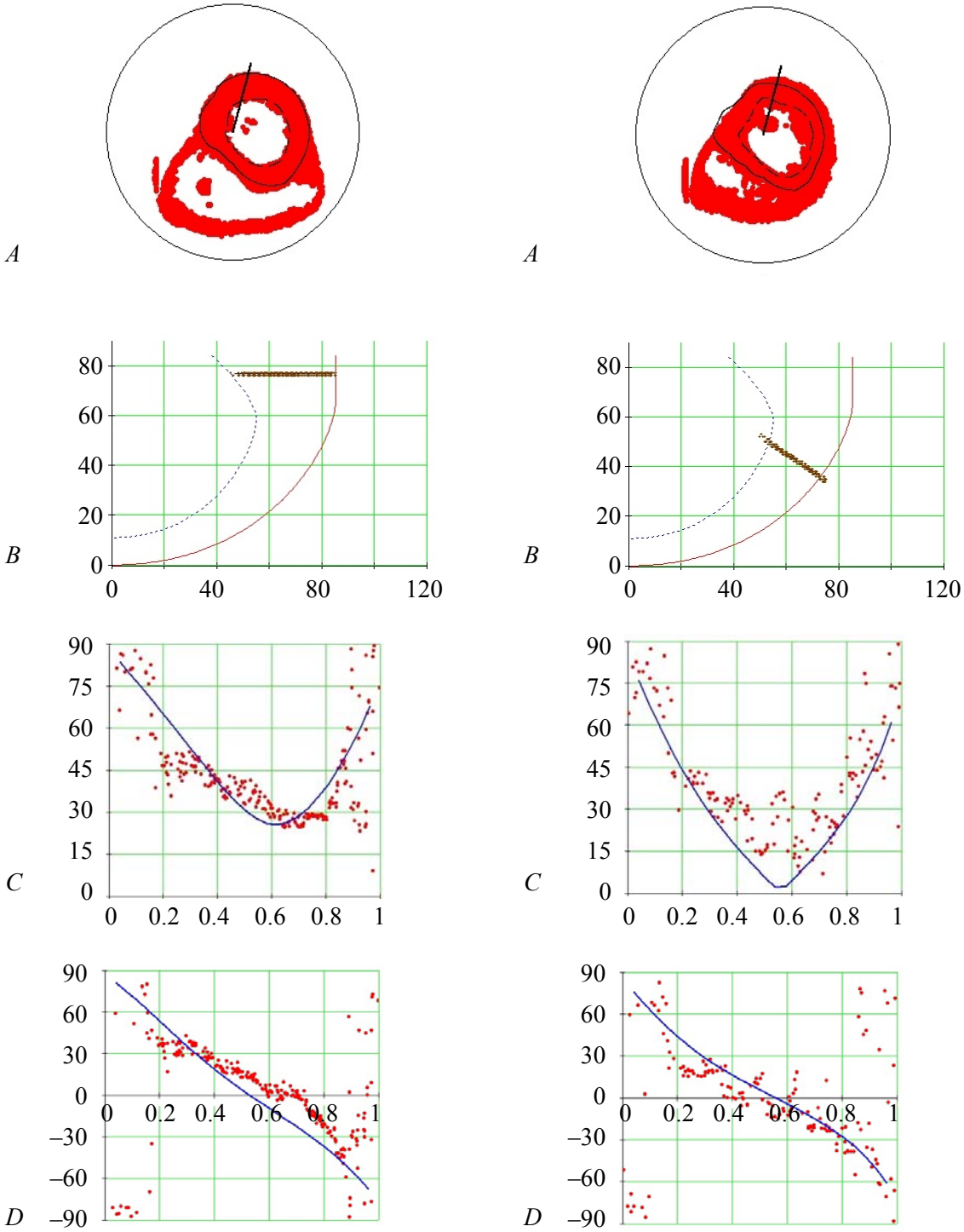

Fig. 13. Fibre angles in the model and in the experimental data. The left ventricle free wall, basal area ($\psi = 5°$), human heart. The conventional signs are the same as in Fig. 7

Fig. 14. Fibre angles in the model and in the experimental data. The left ventricle free wall, middle area ($\psi = 35°$), human heart. The conventional signs are the same as in Fig. 7

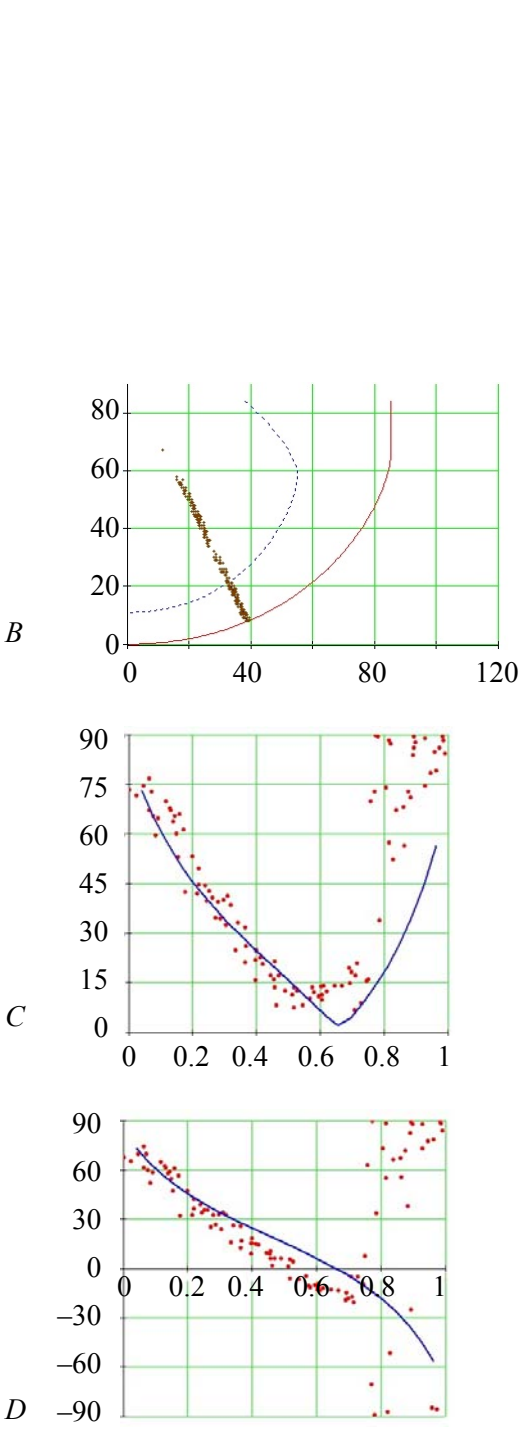

Fig. 15. Fibre angles in the model and in the experimental data. The left ventricle free wall, apical area (ψ=65°), human heart. The conventional signs are the same as in Fig. 7. Horizontal section is not shown

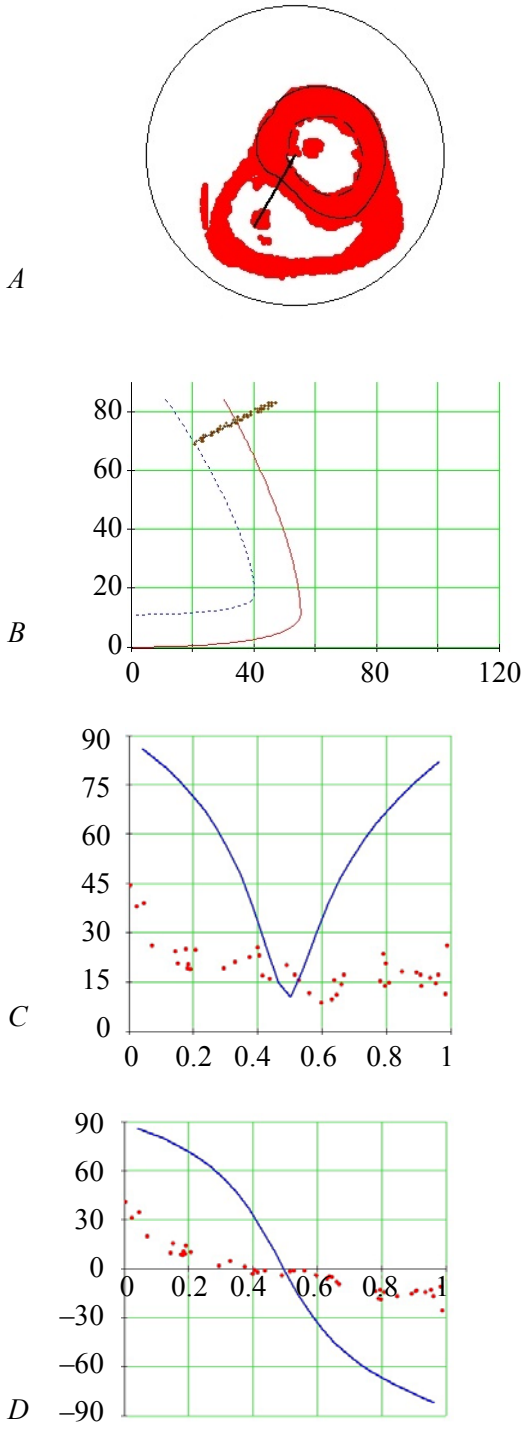

Fig. 16. Fibre angles in the model and in the experimental data. The interventricular septum, basal area (ψ = 5°), human heart. The conventional signs are the same as in Fig. 7

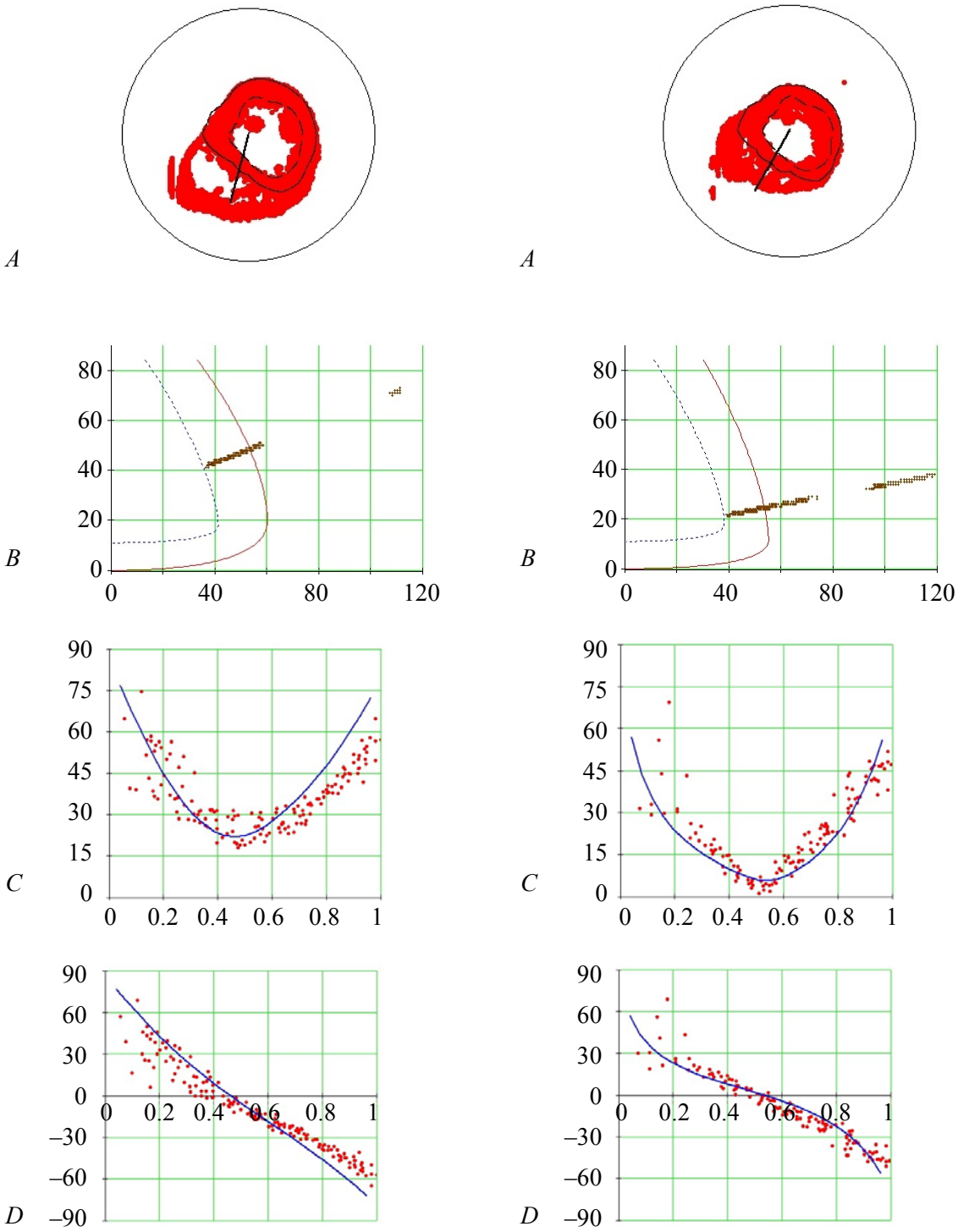

Fig. 17. Fibre angles in the model and in the experimental data. The interventricular septum, middle area ($\psi = 25°$), human heart. The conventional signs are the same as in Fig. 7

Fig. 18. Fibre angles in the model and in the experimental data. The interventricular septum, apical area ($\psi = 45°$), human heart. The conventional signs are the same as in Fig. 7

One can make practically the same statement about the angles at the lower part of left ventricle free wall (Fig. 15). Let us notice only that in the subepicardial wall part, the angle α increases considerably more dramatically than usually, the angle α_1 does not decrease but increase and a great variation of its values can be seen.

In the upper part of interventricular septum (Fig. 16), the angles do not match in the model and in the experimental data.

In the middle and lower interventricular septum parts (Figs. 17 and 18), the model reproduces the angles reasonably accurately.

If one considers the fibres in the radial direction, both our model and the model from [27] imitate the distinctive arrangement of fibres in the ventricular wall ([27], Fig. 14). This arrangement was called the 'Japanese fan' by Streeter ([31], Fig. 42, *C*).

We can conclude that our model adequately reproduces the fibre directions in the left ventricle.

DISCUSSION

This section deals with limitations, ways of verification, usage, and further development of the model constructed.

Limitations

The model adequately reproduces the fibre angles in the upper and middle zones of the left ventricle free wall and in the middle and lower zones of the interventricular septum of human heart (the angles are modelled slightly less accurately in the canine heart). Nevertheless, the data agreement in the apical zone of free wall is only qualitative; in the interventricular septum upper part of human heart, the model yields results that differ totally from the experimental data.

The inaccurate reproduction of the fibre direction angles in the apical left ventricle zone can be explained using Torrent-Guasp's 'unique muscular band' approach. According to this theory (e.g., [34, 18]), the left and right ventricles myocardium forms a single long wrapped muscular band. The left ventricle and interventricular septum together take roughly 75% of the band length, and the right ventricle takes 25% (called the 'right segment'). It is particularly important that the upper part (approximately two thirds) of left ventricle free wall is formed from one band area ('left segment') and the lower one (about one third) is formed from another area ('descending segment') that is not adjacent to the first one. The model reproduces the wrapping of the left segment (exterior upper part of the left ventricle free wall) well, but not the folding of the descending and ascending segments. In the descending segment, the model can reproduce well the fibre directions in the area that is close to the left segment (internal upper part of the left ventricle free wall), its lower middle area (internal lower part of the left ventricle free wall and interventricular septum) and the upper part which is close to the ascending segment (the mid-myocardial left ventricle free wall zone). In the ascending segment, there are two relatively small areas where the tomography data are not reproduced well; one adjoins the aorta, another abuts the apex. The rest of ascending segment corresponds to the external part of left ventricle free wall and interventricular septum; the fibre organization is reproduced well here.

Experimental techniques suitable for the model verification

Currently, a number of experimental methods allows use to measure cardiac fibre directions. One of them is Diffusion Tensor Magnetic Resonance Imaging in which a matrix of water molecule diffusion in the heart is found. The main diffusion directions are identified by the tissue structure [13, 19, 12, 39]. The fibre direction coincides with the matrix

eigenvector, which corresponds to its greatest eigenvalue. The spatial resolution of Diffusion Tensor Magnetic Resonance Imaging reaches 200 microns [8]. Another modern method is the microcomputer tomography, which has a spatial resolution up to 36–70 microns [2]. Both methods yield high-quality data that is needed for computer models.

The scrupulous histological study of the fibres in space [31, 21] must be mentioned when discussing invasive methods of directly measuring the fibre directions. This requires a series of parallel sections of the heart. In each section, the angle of the fibre slope that produces a full pattern of the fibre direction field in the whole heart is gauged. Recently, Smaill et al. developed a method of combined serial high-resolution microscopy [36]. In this method, a series of microscopic sections of the fixed heart was conducted. From these sections, serial high-resolution images were obtained, and, after computerized processing, a consistent cardiac model was formed.

In article [16], quantitative polarized light microscopy is utilized for the analysis of fibres in foetal human heart. The hearts are placed in a pellucid resin, polymerized and sectioned. Thereafter, the elevation and azimuth angles are found with the help of polarized light (see [16] for details).

Comparison with other models

In order to build anatomical computational cardiac models, one can use experimental data from the fibre directions in two ways:

– first, as a discrete dataset in finite element models [40, 11, 41];

– second, for the rule-based models verification [29, 5, 3, 14].

The Laplace–Dirichlet algorithm is one of the recent rule-based techniques, it is described in [3]. The algorithm receives a noisy Diffusion Tensor Magnetic Resonance Imaging-derived fibre orientation field and returns two types of output data: first, transmural and apico-basal directions for the whole myocardium; second, a continuous and smooth fibre orientation field. Peskin [23] obtained a fibre direction field on the basis of mechanical equilibrium principle. Chadwick [7] used concepts of mechanical activity of the heart to construct an anatomic model: he considered a cylindric left ventricle and set a linear dependence of the helix angle on point position in the left ventricle wall. Beyar et al. [4] used the same linear dependence and spherical left ventricle. In 1982, Arts et al. [1] proposed the principle of mechanical adaptation, which allowed calculation of the helix angle distribution. This was used in work [6] by Bovendeerd et al. in which they constructed a model of an ellipsoidal left ventricle and applied a more complex helix angle law, namely a piecewise quadratic law.

The model of left ventricle architecture presented in this article is rule-based and includes the ventricle shape and run of fibres in its wall. The model is substantively connected with Pettigrew's idea of nested spiral surfaces [24], Torrent-Guasp's theory of a unique muscular band [33] and Streeter's anatomical observations represented in his classical work [31]. We obtain cardiac anisotropy by using some common principles, that is, the left ventricle is constructed as a set of similar "spiral" surfaces each of which is defined analytically and represents an image of a semicircle. The mapping of the semicircle consists of two steps. In the first step, the semicircle is transformed into a rectangle in a special coordinate system. The second step maps the special coordinates to cylindrical ones. This map is directly linked with the epicardium and endocardium shape, which is obtained by Diffusion Tensor Magnetic Resonance Imaging, for example. As a result, we obtain spiral surfaces filled by curves (myofibres). These curves are images of the semicircle chords that are parallel to the diameter (Fig. 2).

Besides our model, there are other myocardial models that are based on the idea of wrapping surfaces. Sinha et al. considered [30] a model of one myocardial layer in the form of

a rectangle, which was wrapped around a (truncated) cone. They utilized this unsophisticated model to simulate self-induced waves and to study their disappearance. The waves in Sinha's work revolved around obstacles in the isotropic and anisotropic cases, but there was no association with the real fibre pattern in the ventricles.

To verify the model, we use Diffusion Tensor Magnetic Resonance Imaging experimental data of normal canine and human hearts. The model adequately reproduces both loop-like fibre shape and the 3D arrangement of fibres in the left ventricle wall (Streeter compared the arrangement with Japanese fan).

The model is based on the theoretical postulates of Torrent-Guasp's band conception and gives an appropriate fibre direction field; this is an important argument for the band concept.

Let us compare the model with another rule-based model in which fibre orientation is assigned locally. We compare it with the model from [3] by Bayer et al. We use fibre orientation data from different parts of the left ventricle for comparison. The basis of Bayer's model is the Diffusion Tensor Magnetic Resonance Imaging data of canine heart ventricles. Bayer's model and the experimental data are in agreement, although there is not a full quantitative reproduction of the data (average error in fibre directions is 23°). Bayer's model reproduces fibre anisotropy in the left ventricle basal zone qualitatively better than our model ([3], Fig. 3). Our model yields better results in the middle (by height) left ventricle zone, because we get the specific *s*-like graph of the angle α_1 in the transmural direction (Fig. 8, *D*), and this dependence is linear by definition in Bayer's model. Moreover, the formulae (1) and (2) from the Bayer article make all graphs of the angle α_1 (Figs. 7–12, *D*) independent from latitude and longitude of epicardial normal along which the angle is calculated. Bayer et al. claim that non-linearity of the angle α_1 can be easily embedded in their model, but the anisotropy should necessarily be latitudinally and longitudinally dependent, which is a rather complicated problem. Our model demonstrates this dependence (Figs. 7–12), which reflects the real cardiac fibre pattern, especially in the left ventricle middle zone.

The Bayer model also simplifies the transmural fibre rotation (Japanese fan) by Streeter ([31], Fig. 42 *C*). In the Bayer model, fibres rotate only in one plane and only around one transmural axis. This plane is a tangent plane for surface d = const, where d is a variable from the article [3]. This variable describes point position in the wall (d = 0 on the endocardium and d = 1 on the epicardium). Additionally, if we find the angle α_3, which is defined by Streeter in [31] and reflect fibre direction relative to myocardial layer, the angle is constantly equal to 0, which is a significant simplification. Hence, fibre direction in the wall relative to muscle '*d*-layers' cannot be defined in the Bayer model.

In contrast, this 3D pattern is taken into account in our model, and the fibres on a spiral surface go from the subepicardium to the subendocardium.

Thus, we conclude that both models have their strengths and weaknesses. Additional development of the models would be useful to surmount the limitations.

Further development and usage of the model

The analytical description of the cardiac geometry can be used in developing new numerical methods for the study of electrophysiological and mechanical activity of the left ventricle. The model is an analytical map of a rectangle in space (γ, ψ, φ) to a curvilinear left ventricle; therefore, one can make a numerical scheme on a rectangular area in the coordinates (γ, ψ, φ) (where the boundary conditions can be written in the simplest manner), and we can consider anisotropy by using explicit analytical formulae. The model can also be utilized for the generation of different anisotropic properties of the heart, for alteration of the left ventricle

shape (by change of the model parameters) and for studying their influence on the cardiac electrical and mechanical function.

CONCLUSIONS

An analytical description of the cardiac left ventricle anatomy on basis of Torrent-Guasp's band conception and Pettigrew's spiral surfaces is constructed. The model can be used for band hypothesis verification, for simulating cardiac mechanical function and for various numerical experiments that study the influence of anisotropy on the electrical excitation spread. A good qualitative and – in some left ventricle wall areas – quantitative agreement between the model and experimental data is demonstrated.

ACKNOWLEDGEMENTS

The author would like to thank his scientific supervisors and colleagues from Institute of Mathematics and Mechanics – V.I. Berdyshev and Yu.N. Subbotin, from Institute of Immunology and Physiology Ural Branch of Russian Academy of Sciences – L.B. Katsnelson, V.S. Markhasin and O.E. Solovyova and from University of Ghent (Belgium) – A.V. Panfilov, for their fruitful collaboration in the model discussion.

This work was supported by the Presidium of Ural Branch of Russian Academy of Sciences (project 12-M-14-2009), Ghent University (grant 01SF1511), Institute of Mathematics and Mechanics Ural Branch of Russian Academy of Sciences (youth scientific project), Russian Foundation for Basic Research (grant 13-01-96048) and the Government of Sverdlovsk Region.

REFERENCES

1. Arts T., Veenstra P.C., Reneman R.S. Epicardial deformation and left ventricular wall mechanics during ejection in the dog. *American Journal of Physiology. Heart and Circulatory Physiology*, 1982, vol. 243, no. 12, pp. H379-H390.
2. Aslanidi O.V., Nikolaidou T., Zhao Jichao, Smaill B.H., Gilbert S.H., Holden A.V., Lowe T., Withers P.J., Stephenson R.S., Jarvis J.C., Hancox J.C., Boyett M.R., Zhang H. Application of micro-computed tomography with iodine staining to cardiac imaging, segmentation, and computational model development. *IEEE Transactions on Medical Imaging*, 2013, vol. 32, no. 1, pp. 8-17.
3. Bayer J.D., Blake R.C., Plank G., Trayanova N.A. A novel rule-based algorithm for assigning myocardial fiber orientation to computational heart models. *Ann. Biomed. Eng.*, 2012, vol. 40, no. 10, pp. 2243-2254.
4. Beyar R., Sideman S. A computer study of the left ventricular performance based on fiber structure, sarcomere dynamics, and transmural electrical propagation velocity. *Circ. Res.*, 1984, vol. 55, pp. 358-375.
5. Bishop M.J., Plank G., Burton R.A., Schneider J.E., Gavaghan D.J., Grau V., Kohl P. Development of an anatomically detailed MRI-derived rabbit ventricular model and assessment of its impact on simulations of electrophysiological function. *Am. J. Physiol. Heart. Circ. Physiol.*, 2010, vol. 298, no. 2, pp. H699-H718.
6. Bovendeerd P.H.M., Arts T., Huyghe J.M., van Campen D.H., Reneman R.S. Dependence of local left ventricular wall mechanics on myocardial fiber orientation: a model study. *J. Biomechanics*, 1992, vol. 25, no. 10, pp. 1129-1140.
7. Chadwick R.S. Mechanics of the left ventricle. *Biophysical Journal*, 1982, vol. 39, pp. 279-288.
8. Gilbert S.H., Sands G.B., LeGrice I.J., Smaill B.H., Bernus O., Trew M.L. A framework for myoarchitecture analysis of high resolution cardiac MRI and comparison with diffusion tensor MRI. Annual *International Conference of the IEEE. Engineering in Medicine and Biology Society (EMBC)*, 2012, pp. 4063-4066.
9. Grandi E., Pasqualini F.S., Bers D.M. A novel computational model of the human ventricular action potential and Ca transient. *Journal of Molecular and Cellular Cardiology. Special Issue: Ion Channels*, 2010, vol. 48, no. 1, pp. 112-121.
10. Greenstein J.L., Winslow R.L. Integrative systems models of cardiac excitation-contraction coupling. *Circ. Res*., 2011, vol. 108, pp. 70-84.

11. Gurev V., Lee T., Constantino J., Arevalo H., Trayanova N.A. Models of cardiac electromechanics based on individual hearts imaging data: Image-based electromechanical models of the heart. *Biomech. Model. Mechanobiol.*, 2011, vol. 10, no. 3, pp. 295-306.
12. Helm P., Beg M.F., Miller M.I., Winslow R.L. Measuring and mapping cardiac fiber and laminar architecture using diffusion tensor MR imaging. *Ann. N. Y. Acad. Sci*., 2005, vol. 1047, pp. 296-307.
13. Helm P.A., Tseng H.J., Younes L., McVeigh E.R., Winslow R.L. Ex vivo 3D diffusion tensor imaging and quantification of cardiac laminar structure. *Magnetic Resonance in Medicine*, 2005, vol. 54, pp. 850-859.
14. Hren R. A Realistic Model of the Human Ventricular Myocardium: Application to the Study of Ectopic Activation. PhD thesis. Halifax, Nova Scotia, Canada: Dalhousie University, 1996, 269 p.
15. Hunter P.J., McCulloch A.D., ter Keurs H.E. Modelling the mechanical properties of cardiac muscle. *Prog. Biophys. Mol. Biol*., 1998, vol. 69, pp. 289-331.
16. Jouk P.S., Usson Y., Michalowicz G., Grossi L. Three-dimensional cartography of the pattern of the myofibres in the second trimester fetal human heart. *Anat. Embryol. (Berl.)*, 2000, vol. 202, no. 2, pp. 103-118.
17. Ter Keurs H.E., Shinozaki T., Zhang Y.M., Zhang M.L., Wakayama Y., Sugai Y., Kagaya Y., Miura M., Boyden P.A., Stuyvers B.D., Landesberg A. Sarcomere mechanics in uniform and non-uniform cardiac muscle: a link between pump function and arrhythmias. *Prog. Biophys. Mol. Biol*., 2008, vol. 97, no. 2–3, pp. 312-331.
18. Kocica M.J., Corno A.F., Lackovic V., Kanjuh V.I. The helical ventricular myocardial band of Torrent-Guasp. *Seminars in Thoracic and Cardiovascular Surgery: Pediatric Cardiac Surgery Annual*, 2007, vol. 10, no. 1, pp. 52-60.
19. Lunkenheimer P.P., Redmann K., Kling N., Jiang X., Rothaus K., Cryer C.W., Wübbeling F., Niederer P., Heitz P.U., Ho S.Y., Anderson R.H. Three-dimensional architecture of the left ventricular myocardium. *The Anatomical Record Part A*, 2006, vol. 288, pp. 565-578.
20. Niederer S.A., Hunter P.J., Smith N.P. A quantitative analysis of cardiac myocyte relaxation: a simulation study. *Biophys. J*., 2006, vol. 90, no. 5, pp. 1697-1722.
21. Nielsen P.M.F., LeGrice I.J., Smaill B.H., Hunter P.J. Mathematical model of the geometry and fibrous structure of the heart. *Am. J. Physiol.*, 1991, vol. 260, pp. H1365-H1378.
22. O'Hara T., Virag L., Varro A., Rudy Y. Simulation of the undiseased human cardiac ventricular action potential: Model formulation and experimental validation. *PLoS Comput. Biol*., 2011, vol. 7, no. 5:e1002061.
23. Peskin C.S. Fiber architecture of the left ventricular wall: An asymptotic analysis. *Communications on Pure and Applied Mathematics*, 1989, vol. 42, no. 1, pp. 79-113.
24. Pettigrew J. On the arrangement of the muscular fibers of the ventricular portion of the heart of the mammal. *Proc. Roy. Soc.*, London, 1860, vol. 10, pp. 433-440.
25. Pravdin S.F. Neosesimmetrichnaya model formy i arkhitektoniki levogo zheludochka serdtsa [A non-axisymmetric model of the shape and architecture of heart left ventricle*]. Tezisy dokladov Mezhdunarodnoy (44-y Vserossiyskoy) molodezhnoy shkoly-konferentsii "Sovremennyye problemy matematiki"*. Ekaterinburg, 2013, pp. 131-134 (*in Russian*).
26. Pravdin S.F., Berdyshev V.I., Katsnelson L.B., Solovyova O.E., Markhasin V.S. Staticheskaya matematicheskaya model arkhitektoniki levogo zheludochka serdtsa cheloveka [A static mathematical model of the human heart left ventricle architecture]. *Tezisy dokladov 42-y Vserossiyskoy molodezhnoy shkoly-konferentsii "Sovremennyye problemy matematiki"*. Ekaterinburg, 2011, pp. 311-314 (*in Russian*).
27. Pravdin S.F., Berdyshev V.I., Panfilov A.V., Katsnelson L.B., Solovyova O., Markhasin V.S. Mathematical model of the anatomy and fibre orientation field of the left ventricle of the heart. *Biomedical Engineering Online*, 2013, vol. 54, no. 12, 21 p.
28. Rice J.J., de Tombe P.P. Approaches to modeling crossbridges and calcium-dependent activation in cardiac muscle. *Prog. Biophys. Mol. Biol.*, 2004, vol. 85, no. 2–3, pp. 179-195.
29. Seemann G. Modeling of Electrophysiology and Tension Development in the Human Heart. Ph.D. thesis. Karlsruhe: Universitat Karlsruhe, 2005, 234 p.
30. Sinha S., Stein K.M., Christini D.J. Critical role of inhomogeneities in pacing termination of cardiac reentry. *Chaos: An Interdisciplinary Journal of Nonlinear Science*, 2002, vol. 12, no. 3, pp. 893-902.
31. Streeter D.D.J.R. Gross morphology and fiber geometry of the heart. In: Handbook of Physiology. Sec. 2. Vol. I. Bethesda, Maryland: Am. Physiol. Soc., 1979, pp 61-112.
32. Sulman T., Katsnelson L.B., Solovyova O., Markhasin V.S. Mathematical modeling of mechanically modulated rhythm disturbances in homogeneous and heterogeneous myocardium with attenuated activity of $Na^+ – K^+$ pump. *Bull. Math. Biol*., 2008, vol. 70, no. 3, pp. 910-949.
33. Torrent-Guasp F. The Cardiac Muscle. Madrid: Fundacion Juan March, 1973.

34. Torrent-Guasp F., Kocica M.J., Corno A.F., Komeda M., Carreras-Costa F., Flotats A., Cosin-Aguillar J., Wen H. Towards new understanding of the heart structure and function. *European Journal of Cardio-thoracic Surgery*, 2005, vol. 27, pp. 191-201.
35. Trayanova N.A., Constantino J., Gurev V. Electromechanical models of the ventricles. *Am. J. Physiol. Heart Circ. Physiol.*, 2011, vol. 301, pp. H279-H286.
36. Trew M.L., Caldwell B.J., Sands G.B., LeGrice I.J., Smaill B.H. Three-dimensional cardiac tissue image registration for analysis of in vivo electrical mapping. *Ann. Biomed. Eng*., 2011, vol. 39, no. 1, pp. 235-248.
37. Ten Tusscher K.H., Panfilov A.V. Alternans and spiral breakup in a human ventricular tissue model. *Am. J. Physiol. Heart Circ. Physiol*., 2006, vol. 291, pp. H1088-1100.
38. Ten Tusscher K.H.W.J., Noble D., Noble P.J., Panfilov A.V. A model for human ventricular tissue. *Am. J. Physiol. Heart Circ. Physiol*., 2004, vol. 286, pp. H1573-H1589.
39. Vadakkumpadan F., Arevalo H., Prassl A.J., Chen J., Kickinger F., Kohl P., Plank G., Trayanova N. Image-based models of cardiac structure in health and disease. *Wiley Interdiscip. Rev. Syst. Biol. Med*., 2010, vol. 2, no. 4, pp. 489-506.
40. Vicky Y.W. Modelling In Vivo Cardiac Mechanics using MRI and FEM. PhD thesis. Auckland: Bioengineering Institute, The University of Auckland, New Zealand, 2012.
41. Zhang Y., Liang X., Ma J., Jing Y., Gonzales M.J., Villongco C., Krishnamurthy A., Frank L.R., Nigam V., Stark P., Narayan S.M., McCulloch A.D. An atlas-based geometry pipeline for cardiac Hermite model construction and diffusion tensor reorientation. *Medical Image Analysis*, 2012, vol. 16, no. 6, pp. 1130-1141.

APPENDIX
CALCULATION OF FIBRE DIRECTION IN A POINT

Let us consider a point that has cylindrical coordinates (ρ, φ, *z*). To calculate a fibre direction vector in this point, the following is needed:

1. Use formulae (1)–(3) to numerically find the special coordinates γ and ψ of the point. This problem can be reduced to solving one algebraic equation with one unknown quantity γ, as this needs to express ψ(γ, *z*) in formula (2) and substitute this expression in (1) and (3).

2. Find Cartesian coordinates of the point ($x = \rho \cos \varphi$, $y = \rho \sin \varphi$, z).

3. Differentiate (numerically or analytically) the function ρ(ψ, γ, *φ*) with respect to all arguments and obtain three partial derivatives $\rho_\psi, \rho_\gamma, \rho_\varphi$.

4. The non-normalized vector of fibre direction is:

$$x = \frac{\sin(\pi\gamma)}{\pi - 2\psi} \cdot \left(y\, \varphi^f_{\max} - \cos\varphi \cdot \left(\rho_\gamma + \rho_\varphi\, \varphi^f_{\max} \right) \right) - \cos\varphi \cdot \rho_\psi \cdot \frac{\pi}{2} \cdot \cos(\pi\gamma),$$

$$y = \frac{\sin(\pi\gamma)}{2\psi - \pi} \cdot \left(x\, \varphi^f_{\max} + \sin\varphi \cdot \left(\rho_\gamma + \rho_\varphi\, \varphi^f_{\max} \right) \right) - \sin\varphi \cdot \rho_\psi \cdot \frac{\pi}{2} \cdot \cos(\pi\gamma),$$

$$z = \frac{h^f}{\pi - 2\psi} \cdot \sin(\pi\gamma) \cdot \sin\psi + \left(Z^f - h^f \gamma \right) \cdot \frac{\pi}{2} \cdot \cos(\pi\gamma) \cdot \cos\psi.$$

Received 06 July 2013